Wireless Pers Commun
DOI 10.1007/s11277-011-0231-9

Performance of a Binary PPM Ultra-Wideband Communication System with Direct Sequence Spreading for Multiple Access

Mario E. Magaña · Huaping Liu · Vinod Venkatesan

Abstract In this paper, we present an analysis of the BER performance of an ultra-wideband (UWB) system with pulse position modulation (PPM) for data modulation and direct sequence (DS) spreading for multiple access over indoor lognormal fading channels. A rake receiver is used to combine a subset of the resolvable multipath components using the maximal ratio combining technique. Inter-path and multiple-access interferences are modeled and incorporated into the bit-error-rate expressions. The analytical and simulation results allow one to quantify many critical aspects of a DS-PPM UWB system such as the gain of the optimally spaced signaling scheme over the orthogonal signaling scheme, the potential error floor given a specific channel multipath delay spread and the number of interfering users, tolerance of the system to timing jitter, and impact of user codes.

Keywords Ultra-wideband system · Multiple access · Direct sequence spreading · Pulse position modulation · Multipath fading

1 Introduction

Ultra-wideband (UWB) techniques are attractive for high-rate, low-power communications over short distances. Pulsed UWB systems use short-duration pulses to transmit information. The ultra-wide bandwidth makes the channel highly frequency selective, resulting in a large number of resolvable multipath components at the receiver. The received power is distributed over all these paths, which makes diversity reception a necessity for a reliable communication. Multiple-access communication employing pulsed UWB technologies has drawn significant research interest. Time hopping (TH) multiple access schemes with pulse

M. E. Magaña (✉) · H. Liu · V. Venkatesan
School of Electrical Engineering and Computer Science, Oregon State University, Corvallis, OR 97331, USA
e-mail: magana@eecs.oregonstate.edu

V. Venkatesan
Ikanos Communication Inc, 100 Schultz Drive, Redbank, NJ 07701, USA

Published online: 12 February 2011

position modulation (PPM) and pulse amplitude modulation (PAM) have been reported in literature [1, 2, 4]. Various modulation options for TH UWB systems in terms of their spectral characteristics and hardware complexities have been discussed in [5]. Error performances of TH-PPM UWB systems have been studied in [6, 7], and jam resistance of TH-PPM systems was analyzed in [8]. Direct sequence (DS) spreading is also an attractive method for multiple access in UWB systems. Since pulsed ultra-wideband systems are inherently spread spectrum systems, the use of spreading codes is solely for accommodating multiple users. Performance of a DS-PAM UWB system was analyzed in [3]. In [4, 9], performances of TH-PPM and TH/DS-PAM systems have been compared.

Direct sequence can also be used for multiple access in a PPM UWB system. PPM signaling is attractive because of its ease of implementation. However, spectral lines may be generated by PPM signals. In a DS-PPM system, each symbol is represented by a series of pulses that are pulse-amplitude-modulated by a chip sequence. The chip sequence not only facilitates symbol synchronization of different users' signals in the receiver, but also helps to smooth the discrete spectral lines in a PPM system. Input symbols in DS PPM systems are modulated onto the relative positions of each sequence of pulses. For binary signaling, bits '0' and '1' are transmitted by a sequence of pulses with and without a short time-shift relative to the time reference, respectively. Since a series of pulses are used to represent one symbol, many multipath components are received within the observation window of a particular symbol, causing inter-chip interference. Thus, each symbol at the input of the combiner is corrupted by preceding and following symbols, which eventually limits the performance. Another major factor governing the performance of this system, like any other PPM-based system, is the time-shifts used to represent different symbols. The most commonly used PPM scheme is the orthogonal signaling scheme for which the UWB pulse is orthogonal to its time-shifted version. For any M-ary PPM scheme, there also exists a set of optimal time shifts for which the pulse and its time shifted version reach the minimum correlation value.

The purpose of this paper is to present a semi-analytical method for performance analysis of binary DS-PPM UWB systems over indoor lognormal fading channels. Through this analysis, we will quantify critical system performance metrics including the relative performance of the optimally spaced PPM signaling and the commonly used orthogonal PPM signaling when a traditional rake receiver structure is employed, the potential error floors under different channel multipath delay spread values and number of interfering users, the tolerance of the system to timing jitter, and the impact of different choices of user codes will be established through computer simulation. This paper is organized as follows. Section 2 describes the transmitter, the channel, and the receiver models. Error performance analysis based on a semi-analytical approach is given in Sect. 3. Numerical results are obtained and discussed in Sect. 4, followed by concluding remarks in Sect. 5.

2 System Model

2.1 Transmitter Model

For binary DS PPM systems, information bit '1' is represented by a frame of pulses without any delay and information bit '0' is represented by the same frame of pulses but with a delay τ relative to the time reference. Let us assume that there are U users in the system and the user with index $u = 1$ is the desired user. The transmitted UWB signal of the uth ($u = 1, \ldots, U$) user is represented by

$$s_u(t) = \sqrt{\mathcal{E}_s} \sum_{i=-\infty}^{\infty} \sum_{n=0}^{N_c-1} a_{u,n} w \left\{ t - iT_r - nT_c - \frac{\tau}{2}\left(1 - b_{u,i}\right) \right\} \tag{1}$$

where $\mathcal{E}_s$ is the symbol energy (assumed to be same for all users), $w(t)$ is the UWB pulse assumed to have a nonzero value only for a time period T_p, $a_{u,n} \in \{\pm 1\}$ is the nth chip of the uth user, T_r is the symbol repetition period, T_c is the chip duration, N_c is the number of chips used to represent one symbol, $b_{u,i} \in \{\pm 1\}$ is the ith information bit of the uth user, and τ is the time-shift used in PPM. It is also assumed that $T_c = \epsilon\, T_p$, where ϵ is a positive integer. Except for the spreading code, which is unique for each user, and users' information bits, all other parameters defined above are the same for all users.[1]

To ensure that inter-symbol interference (ISI) is negligible, the guard interval, $T_r - N_c T_c$, between adjacent symbols must be large enough for the range of delay spread values encountered. Let the sequence of pulses used to represent a symbol of the uth user be

$$S_{u,1}(t) = \sum_{n=0}^{N_c-1} a_{u,n} w\left\{t - nT_c\right\} \tag{2a}$$

$$S_{u,0}(t) = S_{u,1}(t - \tau) \tag{2b}$$

where $S_{u,1}(t)$ and $S_{u,0}(t)$ have unit energy, i.e., $\int_{-\infty}^{\infty} S_{u,j}^2(t)dt = 1,\ j = 0, 1$. For the orthogonal signaling scheme, τ_{ortho} is chosen to be such that $\int_{-\infty}^{\infty} S_{u,1}(t) S_{u,1}(t - \tau_{ortho})dt = 0$. In the case of direct sequence spread symbols, the orthogonality condition is met for a number of choices of τ $(0 < \tau < T_r)$, and the minimum of those values is chosen as the time shift. For optimally spaced signaling, the time shift τ is chosen in the range $0 \le \tau \le T_p$ such that the cross correlation between the two symbols is minimized. Thus, τ_{opt} is determined as[2]

$$\tau_{opt} \triangleq \underbrace{\arg\min}_{0 \le \tau \le T_p} \int_{-\infty}^{\infty} S_{u,1}(t) S_{u,1}(t - \tau)dt. \tag{3}$$

2.2 Channel Model

Pulsed UWB signaling gives rise to highly frequency-selective channels. Multipath components tend to arrive in clusters [10–12] and fading for each cluster as well as each ray within the cluster is independent. Although a newer UWB channel model has been recently developed [22], it is very complex to use it to derive analytical results, which is one of our main objectives in this paper. Hence, here we use a modified version of the propagation model adopted by the IEEE802.15.3a committee [10], which is described by

$$h_c(t) = X \sum_{l_c=0}^{L_c-1} \sum_{l_r=0}^{L_r-1} \alpha_{l_c,l_r} \delta(t - T_{l_c} - \tau_{l_c,l_r}) \tag{4}$$

where X is the lognormal shadowing, $\{\alpha_{l_r,l_c}\}$ are the multipath gain coefficients, T_{l_c} is the delay of the l_cth cluster, τ_{l_r,l_c} is the delay of the l_rth multipath component relative to the l_cth

[1] Because of the different pseudo-random codes used for multiple access, the optimal or the orthogonal time-shifts for all users might be slightly different. Such a difference, however, disappears when the code length is large (e.g., greater than 30). For simplicity, the time-shift τ is also assumed to be the same for all users.

[2] Note this choice of the time-shift is optimum in a Guassian channel. It may not be optimum when multiple-access interference cannot be approximated as additional Gaussian noise. It is still of interest to see if this design choice improve the performance over the orthogonal signaling scheme.

cluster arrival time T_{l_c}, and $\delta(t)$ is the Dirac delta function. This model can be simplified as $h_c(t) = \sum_{l=0}^{L-1} \alpha_l \delta(t - \tau_l)$, where $l = l_c L_r + l_r$, $L = L_c L_r$, and $\tau_l = T_{l_c} + \tau_{l_c,l_r}$.

Note that the aforementioned model generates continuous time arrival and amplitude values. Thus, it is very difficult to even provide simulation results if the cluster and path delays are left to be continuous in time, as the received signal waveform must be sampled with an infinitely high frequency in the convolution process. Thus, methods and procedures to discretize the continuous-time model to the desired time resolution without losing the essence of the multipath model are provided in [10]. In the discretized model, both cluster arrival times and ray arrival times are rounded to integer multiples of the desired resolution. This effectively yields a tapped-delay-line [11] model expressed as

$$h(t) = \sum_{l=0}^{L-1} \alpha_l \delta(t - l\Delta\tau) \tag{5}$$

where L is the total number of resolvable multipath components, $\Delta\tau$ is the multipath resolution, and $\alpha_l = \lambda_l \beta_l$ is the fading coefficient corresponding to the lth path. Parameter λ_l takes on the values of 1 and -1 with equal probability and accounts for random pulse inversions that could occur due to reflections [12]. For indoor channels, the magnitude term β_l is lognormally distributed [10, 13]. The minimum multipath resolution in this model is equal to the pulse width T_p.

2.3 Receiver Model

After passing through the channel, each user's signal arrives at the receiver as multiple independently faded copies. The received signal with U users in the system, neglecting shadowing effects, is expressed as

$$\begin{aligned} r(t) &= \sum_{u=1}^{U} \sum_{l=0}^{L-1} \alpha_{u,l} s_u(t - l\Delta\tau) + \eta(t) \\ &= \sum_{l=0}^{L-1} \alpha_{1,l} s_1(t - l\Delta\tau) + \sum_{u=2}^{U} \sum_{l=0}^{L-1} \alpha_{u,l} s_u(t - l\Delta\tau) + \eta(t) \end{aligned} \tag{6}$$

where $\eta(t)$ is the additive white Gaussian noise process with a two-sided power spectral density (PSD) of $N_0/2$ and $\alpha_{u,l}$ represents the channel coefficient of the lth path experienced by the uth user's signal. Since the large guard interval between adjacent symbols as mentioned in Sect. 2.1 results in negligible ISI, the received signals can be processed separately for each symbol. Therefore, the ensuing analysis applies to both synchronous and asynchronous reception by simply applying the correct cross-correlation values among the asynchronous user codes in calculating multiple-access interference (MAI). If user 1 is the desired user, the second term on the right-hand side of Eq. (6) is the MAI from $U - 1$ interfering users.

The optimal receiver for the single-user PPM system is a correlation receiver with a template waveform [14]

$$\Delta_u(t) = S_{u,1}(t) - S_{u,0}(t). \tag{7}$$

Although this receiver is not optimum when MAI is present, it is adopted in this paper because of its simplicity. A rake receiver, a uniform tapped-delay-line demodulator [11, 15] with maximal ratio combining, is applied to capture energy contained in resolvable multipath components.

3 Error Performance Analysis

We focus on the detection of the first bit of the desired user ($u = 1$). Without loss of generality, we assume that the transmitted bit is a '1', i.e., $s_1(t) = \sqrt{\mathcal{E}_s} S_{1,1}(t)$ during the time interval $0 \le t \le T_r$. With the large guard interval between adjacent symbols as mentioned in Sect. 2.1, there is no ISI. The interfering users' signal is assumed to have similar characteristics to the desired user's signal with respect to symbol period, length of spreading code, pulse width, and chip period.

For simplicity of notation, the index for the desired user ($u = 1$) will be omitted for some variables. Let the autocorrelation function of $S_{u,1}(t)$ be

$$\gamma_u(v) \triangleq \int_{-\infty}^{\infty} S_{u,1}(t) S_{u,1}(t - v) dt. \tag{8}$$

and let

$$f_{u,j}(t, l) \triangleq S_{u,j}(t - l\Delta\tau) \Delta_1^{(k)}(t),$$

where $\Delta_1^{(k)}(t) = \Delta_1(t - k\Delta\tau)$ is the template waveform corresponding to the kth finger of the desired user.

Assuming knowledge of the desired user's channel coefficients, i.e.,

$$\boldsymbol{\alpha}_1 = \left[\alpha_{1,0} \; \alpha_{1,1} \cdots \alpha_{1,L-1} \right]',$$

then, the observed signal at the output of the kth finger of the user of interest (user 1) receiver is the sum of the signal, inter-path interference (self-noise), MAI, and additive noise components, i.e.

$$Y_{k|\text{“1”},\boldsymbol{\alpha}_1} = Y_{s,k|\text{“1”},\boldsymbol{\alpha}_1} + Y_{sn,k|\text{“1”},\boldsymbol{\alpha}_1} + Y_{mai,k|\boldsymbol{\alpha}_1} + Y_{\eta,k|\boldsymbol{\alpha}_1}. \tag{9}$$

where

$$\begin{aligned} Y_{s,k|\text{“1”},\boldsymbol{\alpha}_1} &= \alpha_{1,k}^2 \sqrt{\mathcal{E}_s} \int_0^{T_r} f_{1,1}(t, k) dt \\ &= \alpha_{1,k}^2 \sqrt{\mathcal{E}_s} \left[1 - \gamma_1(\tau) \right] \end{aligned} \tag{10a}$$

$$Y_{sn,k|\text{“1”},\boldsymbol{\alpha}_1} = \sqrt{\mathcal{E}_s} \alpha_{1,k} \sum_{\substack{l=0 \\ l \ne k}}^{L-1} \alpha_{1,l} \int_0^{T_r} f_{1,1}(t, l) dt \tag{10b}$$

$$Y_{mai,k,|\boldsymbol{\alpha}_1} = \sqrt{\mathcal{E}_s} \alpha_{1,k} \sum_{u=2}^{U} \sum_{l=0}^{L-1} \alpha_{u,l} \int_0^{T_r} f_{u,j}(t, l) dt \tag{10c}$$

$$Y_{\eta,k,|\boldsymbol{\alpha}_1} = \alpha_{1,k} \int_0^{T_r} \eta(t) \Delta_1^{(k)}(t) dt \tag{10d}$$

where $j = 0$ or 1 corresponds to the symbol transmitted by the uth user. The inter-path interference as shown in (10b) has $(L - 1)$ terms. Since $S_{u,1}(t)$ given in (2a) consists of N_c pulses (pulse width $T_p < T_c$) that are T_c apart, the autocorrelation function $\gamma_u(v)$ is non-zero only for certain values of the argument v. Non-zero values of $\gamma_u(v)$ are centered around the

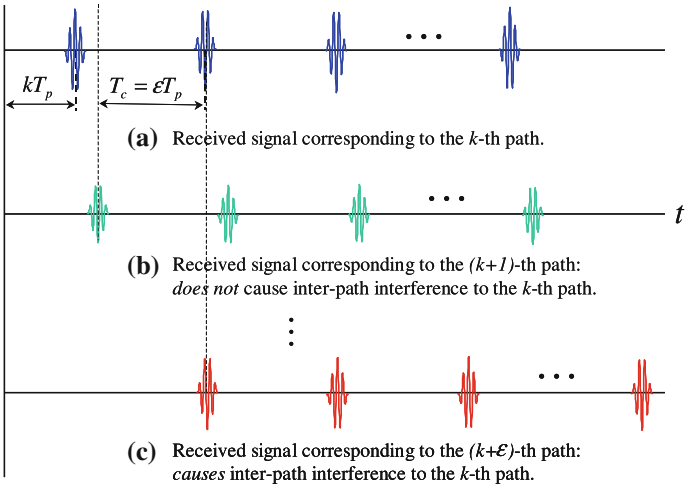

Fig. 1 Illustration of inter-path interference

local minima's and maxima's of $\gamma_u(v)$ that are T_c apart. Hence, inter-path interference is caused by multipath components which are spaced at integer multiples of T_c from paths that arrives before and after the kth path. This scenario is illustrated in Fig. 1.

The error performance analysis becomes mathematically tractable if the number of paths combined by the rake is less than the ratio $\epsilon = T_c/T_p$. This ensures that interference is caused only by the min $\left\{N_c - 1, \left\lfloor \frac{L-k}{\epsilon} \right\rfloor\right\}$ paths arriving at integer multiples of T_c after the kth path, where $\lfloor \cdot \rfloor$ denotes the integer part of the argument. Considering implementation complexity, the rake receiver in practical systems is unlikely able to combine more than ϵ (e.g., $\epsilon = 13$) fingers. Thus, even with this condition, the analysis results still have practical values. Under this condition, the conditional inter-path interference term, $Y_{sn,k|\text{“1”},\boldsymbol{\alpha}_1}$, can be simplified as

$$Y_{sn,k|\text{“1”},\quad \boldsymbol{\alpha}_1 = \sqrt{\mathcal{E}_s}\alpha_{1,k}\boldsymbol{\alpha}_{1,k}'\boldsymbol{\gamma}_1} \tag{11}$$

where $\{\cdot\}'$ denotes transpose and

$$\begin{aligned} \boldsymbol{\alpha}_{1,k} &= \left[\alpha_{1,k+\epsilon},\ \alpha_{1,k+2\epsilon},\ \ldots,\ \alpha_{1,k+(N_c-1)\epsilon}\right]' \\ \boldsymbol{\gamma}_1 &= \begin{bmatrix} \gamma_1(T_c) - \gamma_1(T_c - \tau) \\ \gamma_1(2T_c) - \gamma_1(2T_c - \tau) \\ \vdots \\ \gamma_1([N_c-1]T_c) - \gamma_1([N_c-1]T_c - \tau) \end{bmatrix} \end{aligned} \tag{12}$$

are $(N_c - 1) \times 1$ vectors.

The codes of interfering users are assumed to be independent of each other. MAI can be modeled in a way similar to the modeling of inter-path interference. The additive noise component is still a zero-mean Gaussian RV whose variance depends on $\alpha_{1,k}$. The kth path to the combiner is expressed as $Y_{k|\text{“1”},\boldsymbol{\alpha}_1} = Y_{s,k|\text{“1”},\boldsymbol{\alpha}_1} + Y_{sn,k|\text{“1”},\boldsymbol{\alpha}_1} + Y_{mai,k|\boldsymbol{\alpha}_1} + Y_{\eta,k|\boldsymbol{\alpha}_1}$ and is a random variable. Variables $Y_{sn,k|\text{“1”},\boldsymbol{\alpha}_1}$, $Y_{mai,k|\boldsymbol{\alpha}_1}$ and $Y_{\eta,k|\boldsymbol{\alpha}_1}$ are zero-mean independent RVs, i.e., $E\{Y_{sn,k|\text{“1”},\boldsymbol{\alpha}_1}\} = E\{Y_{mai,k|\boldsymbol{\alpha}_1}\} = E\{Y_{\eta,k|\boldsymbol{\alpha}_1}\} = 0$ and $E\{Y_{sn,k|\text{“1”},\boldsymbol{\alpha}_1} Y_{\eta,k|\boldsymbol{\alpha}_1}\} = 0$, $E\{Y_{sn,k|\text{“1”},\boldsymbol{\alpha}_1} Y_{mai,k|\boldsymbol{\alpha}_1}\} = 0$, $E\{Y_{mai,k|\boldsymbol{\alpha}_1 Y_{\eta,k|\boldsymbol{\alpha}_1}} = 0$, where $E\{\cdot\}$ denotes statistical

expectation. Taking the expectation with respect to $\boldsymbol{\alpha}_1$, the mean and variance of $Y_{k|\text{“1”},\boldsymbol{\alpha}_1}$ can be determined as

$$E\left\{Y_{k|\text{“1”},\boldsymbol{\alpha}_1}\right\} = Y_{s,k|\text{“1”}} = E\left\{\alpha_{1,k}^2\right\}\sqrt{\mathcal{E}_s}\left[1-\gamma_1(\tau)\right] \tag{13}$$

$$\begin{aligned} Var\left\{Y_{k|\text{“1”},\boldsymbol{\alpha}_1}\right\} &= Var\left\{Y_{s,k|\text{“1”},\boldsymbol{\alpha}_1}\right\} + Var\left\{Y_{sn,k|\text{“1”},\boldsymbol{\alpha}_1}\right\} \\ &\quad + Var\left\{Y_{mai,k|\boldsymbol{\alpha}_1}\right\} + Var\left\{Y_{\eta,k|\boldsymbol{\alpha}_1}\right\}. \end{aligned} \tag{14}$$

The variance of the signal component is found to be

$$Var\left\{Y_{s,k|\text{“1”},\boldsymbol{\alpha}_1}\right\} = \left[E\left\{\alpha_{1,k}^4\right\} - (E\alpha_{1,k}^2\})^2\right]\mathcal{E}_s\left[1-\gamma_1(\tau)\right]^2 \tag{15}$$

The variance of the self-noise term is found by squaring $Y_{sn,k|\text{“1”},\boldsymbol{\alpha}_1}$ and taking its expected value. Now, $Y^2_{sn,k|\text{“1”},\boldsymbol{\alpha}_1}$ is a function of $\alpha_{1,i}\alpha_{1,j}$. Since the multipath components are assumed to be independent, $E\{\alpha_{1,i}\alpha_{1,j}\} = 0$ for $i \neq j$. Hence, the variance of the self-noise term simplifies to

$$Var\left(Y_{sn,k|\text{“1”},\boldsymbol{\alpha}_1}\right) = \mathcal{E}_s E\{\alpha_{1,k}^2\} E\,\boldsymbol{\alpha}_{1,k}^{(2)'}\}\boldsymbol{\Gamma}_1 \tag{16}$$

where $(N_c-1)\times 1$ vectors $\boldsymbol{\alpha}_{1,k}^{(2)}$ and $\boldsymbol{\Gamma}_1$ are given as

$$\begin{aligned} \boldsymbol{\alpha}_{1,k}^{(2)} &= \left[\alpha_{1,k+\epsilon}^2,\, \alpha_{1,k+2\epsilon}^2,\, \ldots,\, \alpha_{1,k+(N_c-1)\epsilon}^2\right]' \\ \boldsymbol{\Gamma}_1 &= \begin{bmatrix} \{\gamma_1(T_c) - \gamma_1(T_c-\tau)\}^2 \\ \{\gamma_1(2T_c) - \gamma_1(2T_c-\tau)\}^2 \\ \vdots \\ \{\gamma_1([N_c-1]\,T_c) - \gamma_1([N_c-1]\,T_c-\tau)\}^2 \end{bmatrix}. \end{aligned} \tag{17}$$

It should be mentioned that in Eqs. (12) and (17) the autocorrelation values do not depend on k, the index of the path combined by the receiver. Following a similar procedure, the variance of MAI can also be obtained. Let the cross-correlation function of $S_{1,1}(t)$ and $S_{u,j}(t)$, where $j = 0, 1$ depending on the symbol transmitted by the uth user, be

$$\tilde{\gamma}_u(v) \triangleq \int_{-\infty}^{\infty} S_{1,1}(t)S_{u,j}(t-v)dt. \tag{18}$$

Clearly, the cross-correlation function is dependent on the code of the interfering user and the symbol transmitted by that user. Hence, the cross correlation function must be averaged over user codes as well as transmitted symbols of interfering users. The variance of the MAI term is of the form

$$Var\left(Y_{mai,k|\boldsymbol{\alpha}_1}\right) = \mathcal{E}_s E\left\{\alpha_{1,k}^2\right\}\sum_{u=2}^{U} E\left\{\tilde{\boldsymbol{\alpha}}_{u,k}^{(2)\prime}\right\}\tilde{\boldsymbol{\Gamma}}_u \tag{19}$$

where $N_c \times 1$ vectors $\tilde{\boldsymbol{\alpha}}_{u,k}^{(2)}$ and $\tilde{\boldsymbol{\Gamma}}_u$ are given as

$$\tilde{\boldsymbol{\alpha}}_{u,k}^{(2)} = \left[\alpha_{u,k}^2,\ \alpha_{u,k+\epsilon}^2,\ \ldots,\ \alpha_{u,k+(N_c-1)\epsilon}^2\right]'$$
$$\tilde{\boldsymbol{\Gamma}}_u = \begin{bmatrix} \{\tilde{\gamma}_u(0) - \tilde{\gamma}_u(\tau)\}^2 \\ \{\tilde{\gamma}_u(T_c) - \tilde{\gamma}_u(T_c - \tau)\}^2 \\ \vdots \\ \{\tilde{\gamma}_u([N_c - 1]\,T_c) - \tilde{\gamma}_u([N_c - 1]\,T_c - \tau)\}^2 \end{bmatrix}. \tag{20}$$

Vector $\tilde{\boldsymbol{\Gamma}}_u$ represents the cross-correlation vector of the interfering users' signal with the desired user's signal. Since the channel statistics are the same for all users, the sum in Eq. (19) can be replaced by a multiplicative factor $(U-1)$ when the autocorrelation vector is averaged over many user codes and transmitted bits. This implies that the variance of the MAI components from all users are the same. The variance of the zero-mean additive noise term can be obtained as $Var\left(Y_{\eta,k|\boldsymbol{\alpha}_1}\right) = E\{\alpha_{1,k}^2\} E\left\{\iint_0^{T_r} \eta(t)\Delta_1^{(k)}(t)\eta(q)\Delta_1^{(k)}(q)dtdq\right\}$.

By interchanging the order of the two linear operators and applying $E\{\eta(t)\eta(q)\} = \frac{N_0}{2}\delta(t-q)$, we obtain the variance of the noise term as

$$Var\left(Y_{\eta,k|\boldsymbol{\alpha}_1}\right) = E\left\{\alpha_{1,k}^2\right\} N_0\big[1 - \gamma_1(\tau)\big]. \tag{21}$$

Using the propagation model presented in [12] and modifying it appropriately, $20\log_{10}(\alpha_{u,k})$ is Gaussian with mean $\mu_{u,k}$ and variance σ^2 given by

$$\mu_{u,k} = \frac{10\ln(\Omega_0) - 10\tau_{u,k}/\gamma}{\ln(10)} - \frac{(\sigma_1^2 + \sigma_2^2)\ln(10)}{20}$$

$$\sigma^2 = \sigma_1^2 + \sigma_2^2.$$

Moreover,

$$E\left\{\alpha_{u,k}^2\right\} = \Omega_0 e^{-\tau_{u,k}/\gamma} \tag{22}$$
$$E\left\{\alpha_{u,k}^4\right\} = e^{\left(\frac{\ln(10)}{10}\sigma\right)^2}\left(E\left\{\alpha_{u,k}^2\right\}\right)^2, \tag{23}$$

where Ω_0 is the mean energy of the first path and γ is the ray decay factor.

Assuming $K\,(K < \epsilon)$ out of L resolvable paths are combined by the rake receiver, the decision statistic at the output of the combiner is expressed as

$$\begin{aligned} Z|\text{“1”},\boldsymbol{\alpha}_1 &= \sum_{k=0}^{K-1} Y_{k|\text{“1”},\boldsymbol{\alpha}_1} \\ &= \sum_{k=0}^{K-1} Y_{s,k|\text{“1”},\boldsymbol{\alpha}_1} + \sum_{k=0}^{K-1} Y_{sn,k|\text{“1”},\boldsymbol{\alpha}_1} + \sum_{k=0}^{K-1} Y_{mai,k|\boldsymbol{\alpha}_1} + \sum_{k=0}^{K-1} Y_{\eta,k|\boldsymbol{\alpha}_1}. \end{aligned}$$

As mentioned earlier, under the assumption that $\{\alpha_{1,0}, \alpha_{1,1}, \ldots, \alpha_{1,K-1}\}$ is known at the receiver, the first term of $Z|\text{“1”},\boldsymbol{\alpha}_1$ is the signal component, the second and third terms are, respectively, the self-noise and MAI components from all the paths. The self-noise and MAI terms for the kth path combined by the rake ($Y_{sn,k|\text{“1”},\boldsymbol{\alpha}_1}$ and $Y_{mai,k|\boldsymbol{\alpha}_1}$) are sums of RVs whose magnitude is lognormal with random pulse inversions.

It is well known that for TH-PPM systems the approximation of MAI as a Gaussian RV based on the central limit argument could lead to very poor performance results (e.g., see [16–18]), especially when the number of users is small. However, the DS-PPM system being addressed in this paper is different from the TH-PPM system in that each bit is represented by N_c chips. Thus, both $Y_{sn,k|\text{“1”},\boldsymbol{\alpha}_1}$ and $Y_{mai,k|\boldsymbol{\alpha}_1}$ are the sum of a large number of nearly independent and identically distributed (i.i.d.) terms.[3] Therefore, it is appropriate to apply the central limit theorem to approximate the statistics of $Y_{sn,k|\text{“1”},\boldsymbol{\alpha}_1}$ and $Y_{mai,k|\boldsymbol{\alpha}_1}$. To justify this claim, Fig. 2 shows the probability density function (PDF) of a sum of lognormal random variables with random pulse inversions, for $n = 1,\ 2,\ 4$ and 6 elements in the sum. Because multipath components are independent of one another, the PDF was obtained by convolving the PDFs of the individual elements in the sum. Clearly, the Gaussian approximation to the sum of lognormal random variables with random pulse inversions is justified when the number of elements in the sum is at least 6. In practical scenarios and the analysis in this paper, the number of elements in the sum for the MAI term is much greater than 6, thus justifying the Gaussian approximation of the self-noise and MAI terms. The fourth term, which is the additive noise component, is a zero mean Gaussian RV. Different paths to the combiner are mutually independent because noise and interference in different paths are also independent of each other. Hence $Z|\text{“1”},\boldsymbol{\alpha}_1$ is a Gaussian RV with a mean and variance that are equal to the sum of the means and variances of all the paths. Thus, mean and variance of $Z|\text{“1”},\boldsymbol{\alpha}_1$ are given by

$$\mu_{Z|\text{“1”},\boldsymbol{\alpha}_1} = \sqrt{\mathcal{E}_s}\left[1-\gamma_1(\tau)\right]\sum_{k=0}^{K-1} E\{\alpha_{1,k}^2\} \tag{24}$$

$$\begin{aligned}\sigma^2_{Z|\text{“1”},\boldsymbol{\alpha}_1} &= \sum_{k=0}^{K-1} Var\left\{Y_{k|\text{“1”},\boldsymbol{\alpha}_1}\right\} \\ &= \sum_{k=0}^{K-1}\Big[Var\left\{Y_{s,k|\text{“1”},\boldsymbol{\alpha}_1}\right\} + Var\left\{Y_{sn,k|\text{“1”},\boldsymbol{\alpha}_1}\right\} \qquad (25)\\ &\quad + Var\left\{Y_{mai,k|\boldsymbol{\alpha}_1}\right\} + Var\left\{Y_{\eta,k|\boldsymbol{\alpha}_1}\right\}\Big]. \qquad (26)\end{aligned}$$

Figure 3 shows the theoretical (obtained by convolution) and the approximated PDFs of the self-noise with different number of rake fingers.

When the value of the combiner output $Z|\text{“1”},\boldsymbol{\alpha}_1$ is less than 0, a wrong decision is made. The probability of error can be obtained as $Q\left(\mu_{Z|\text{“1”},\boldsymbol{\alpha}_1}/\sqrt{\sigma^2_{Z|\text{“1”},\boldsymbol{\alpha}_1}}\right)$ where $Q(\cdot)$ is the Q-function defined as $Q(x) = \int_x^\infty \frac{1}{\sqrt{2\pi}} e^{-x^2/2} dx$. Specifically, $P_{e|\text{“1”}}$ is expressed as

$$P_{e|\text{“1”}} = Q\left(\sqrt{\frac{\mathcal{E}_s\left[1-\gamma_1(\tau)\right]^2 {\varphi_1}^2}{\sum_{k=0}^{K-1} Var\{Y_{k|\text{“1”},\boldsymbol{\alpha}_1}\}}}\right) \tag{27}$$

where $\varphi_1 = \sum_{k=0}^{K-1} E\left\{\alpha_{1,k}^2\right\}$.

Typically it is impossible to find the exact closed-form expression for the characteristic function of the MAI. Thus, in the study of a TH-PPM system in [16] an approximate

[3] The reason for these terms being only nearly i.i.d. is that the channel coefficients for the K paths may have slightly different average powers.

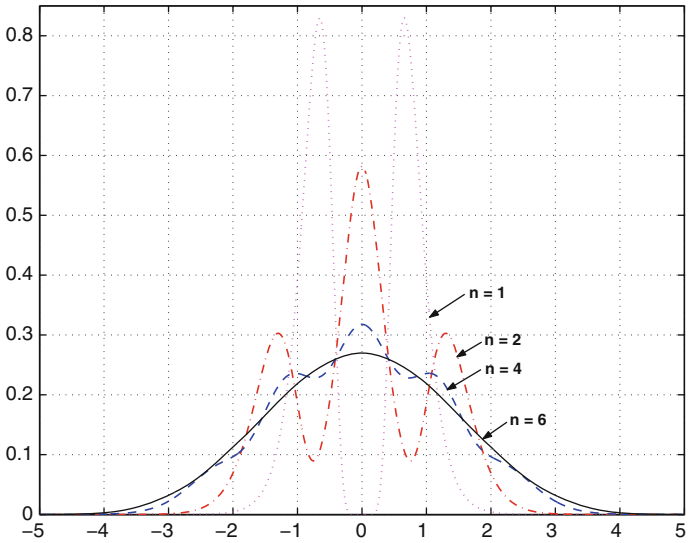

Fig. 2 Gaussian approximation to a sum of random variables whose magnitude is lognormal with random pulse inversions

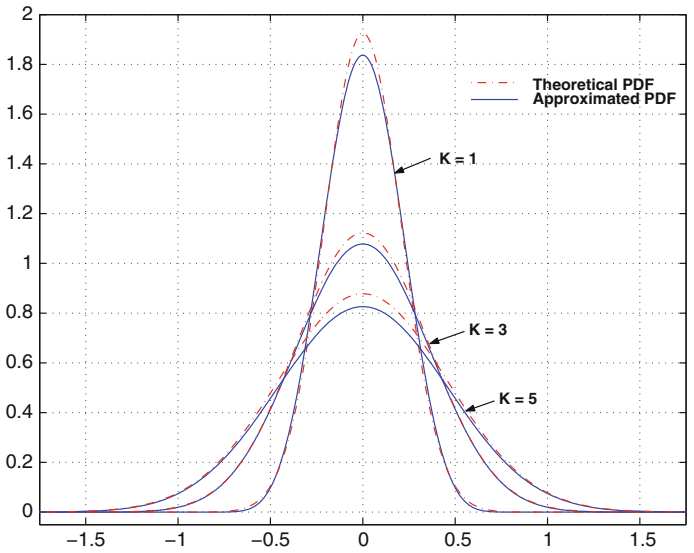

Fig. 3 Approximated and theoretical PDFs of self-noise for different K

characteristic function for the MAI term in the *absence* of multipath fading was given. For the problem being addressed, the self-noise term, the MAI term, and frequency-selective lognormal fading must be dealt with simultaneously.

4 Numerical Results and Discussion

Numerical results are provided in this section to quantify critical performance metrics of DS-PPM UWB systems in lognormal fading environments. Specifically, error performances with different system parameters, error performances under different channel parameters, and tolerance of the system to timing jitters will be evaluated using the model and analysis given in Sect. 3. Waveform based simulation results are obtained to verify the accuracy of the semi-analytical results derived in this paper.

4.1 Setup for Numerical Examples

For all numerical examples, the channel is assumed to have an exponentially decaying multipath intensity profile and the receiver is assumed to have perfect knowledge of the channel coefficients (only those to be combined by the rake) of the desired user. The total number of resolvable paths (L) and the power decay factor (ρ) are obtained using the channel root-mean-square (RMS) delay spread as described in [19]. For a typical indoor environment, the channel standard deviation σ is in the range of 3–5 dB. All paths whose average power is within 15 dB of that of the strongest path are considered. For an RMS delay spread of 20 ns and $T_p = 0.5$ ns, the total number of resolvable paths was obtained to be $L = 179$ with a corresponding power decay factor $\rho = 0.019$. A truncated Gaussian monocycle [8] is applied in simulations and all users (desired and interfering users) have the same bit energy. The sum of power of all paths that are combined by the rake is normalized to unity. Thus, for a given signal-to-noise ratio (SNR), the variance of AWGN is obtained as $N_0/2 = 10^{-\mathrm{SNR}/10}$. User codes of length 32, $\epsilon = 13$, data rate of 2.4 Mbps per user (includes a guard interval of 208 ns), channel RMS delay spread of $\tau_{rms} = 20$ ns, and $\sigma = 3$ dB are adopted in all examples unless explicitly specified otherwise. Unless specified explicitly, the pseudo-random generator provided by MATLAB with its default seed is used to generate the spreading code for the desired user.

4.2 The Impact of System Parameters

Analytical (solid lines with marks) and simulated (dotted lines without marks) error performance curves for a single-user and a multiple-user system with optimally spaced signaling are shown in Fig. 4. For the two sets of system parameters chosen, simulation results match very well with the analytical results.[4] It is also observed that an error floor appears at high $E_b/\mathcal{N}_0$ values because of the inter-path interference. The analytical curves shown are for a system with a low diversity order ($K = 2$ and 3). Although the method presented can be applied to analyze the receiver performance with any diversity order, obtaining analytical curves for higher diversity orders ($K > 3$) becomes computationally intensive since it involves numerical integration of many orders. In the rest of this section, BER curves with more than $K = 3$ fingers will not be accompanied by their corresponding analytical curves.

To assess the performance improvement of the optimally spaced scheme over that of the orthogonal signaling scheme, we plotted SNR versus BER curves for a single-user system with different K in Fig. 5. It is observed that with the set of system parameters and channel parameters chosen, the optimally spaced scheme performs approximately 2 dB better than the orthogonal scheme at a BER of 10^{-4}.

[4] The simulated and analytical curves basically overlap with each other, and are not distinguishable in Fig. 4.

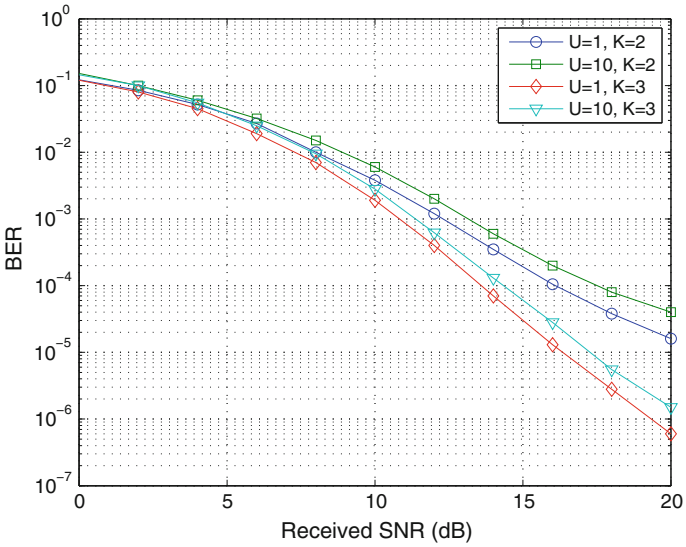

Fig. 4 Comparison of analytical and simulated BER performance with optimally spaced signaling, single and multiple user scenarios

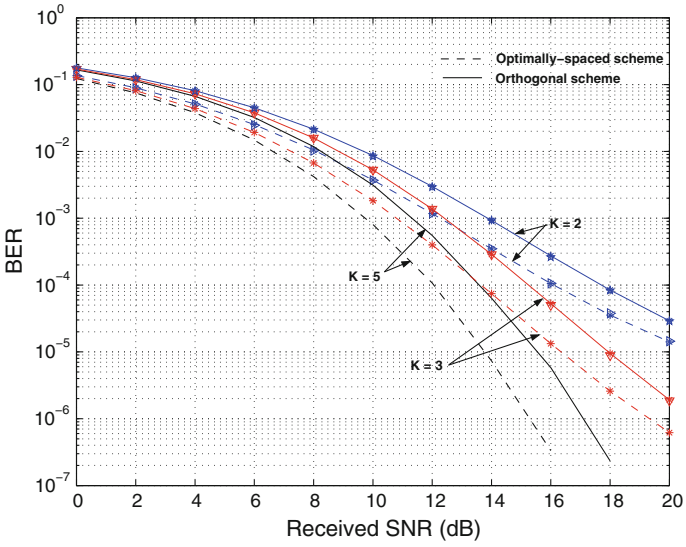

Fig. 5 BER Performance comparison of the optimal (*dashed lines*) and the orthogonal signalling (*solid lines*) schemes (simulation results are plotted with *markers*, $U = 1$)

From the analysis given in Sect. 3, it is clear that the performance of such a system depends on the auto-correlation properties of the user code, which determines the amount of self-noise, just like in a conventional direct-sequence code-division multiple-access (CDMA) system. The MAI component is not only determined by the number of interferers, but also by the cross-correlation properties between the interfering users' signals and the desired user's signal expressed in (20). To avoid the dependency of system performance on specific interfering

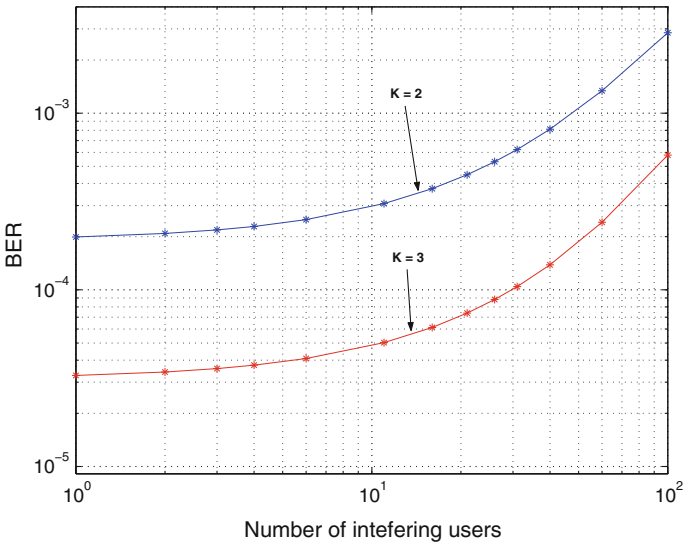

Fig. 6 BER Performance as a function of number of users in a multi-user system at fixed SNR (SNR = 15 dB)

users' codes, the cross-correlation vector given in Eq. (20) is obtained by averaging over a number of random user codes and transmitted symbols of interfering users. The effect of MAI on the error performance of a multi-user system is shown in Fig. 6. BER curves as a function of the number of interfering users ($U-1$) are given for an SNR of 15 dB and $K = 2$ and 3. When the number of interfering users is in the range of 0–20, performance degradation is mild with an increase in U. When the number of interfering users are further increased (e.g., greater than 20), BER deteriorates significantly as the number of interfering users increases.

As seen from Eqs. (16) and (17), performance of this system also depends on the spreading code of the desired user and its auto-correlation properties. The performances could be largely different for different pseudo random codes applied. Figure 7 shows three different analytical BER curves of the optimally spaced scheme with $K = 3$. These curves correspond to performances with different user codes generated by pseudo-random generators with different initial seeds. The pseudo-random generator provided by MATLAB was used and the seeds were 20024, 100, 24, corresponding approximately to the best, the medium, and the worst cases, respectively. Examining the these codes, we found that the code obtained using the first seed has very low off-peak auto-correlation values especially at near the correlation peak, whereas the code obtained using the last seed has very high off-peak auto-correlation values. As clearly seen from (17), the non-zero off-peak autocorrelation of user codes affects the amount of self-noise, which in turn affects the system performance.

4.3 The Impact of Channel Parameters

Figure 8 illustrates the performance of a single-user system that combines 3 paths ($K = 3$) with the optimally spaced scheme for different standard deviation values (σ) of the channel. The system reaches an error floor at high SNR values. A smaller σ results in a lower error floor, and it is found that the impact of σ on the error performance is significant for the set of

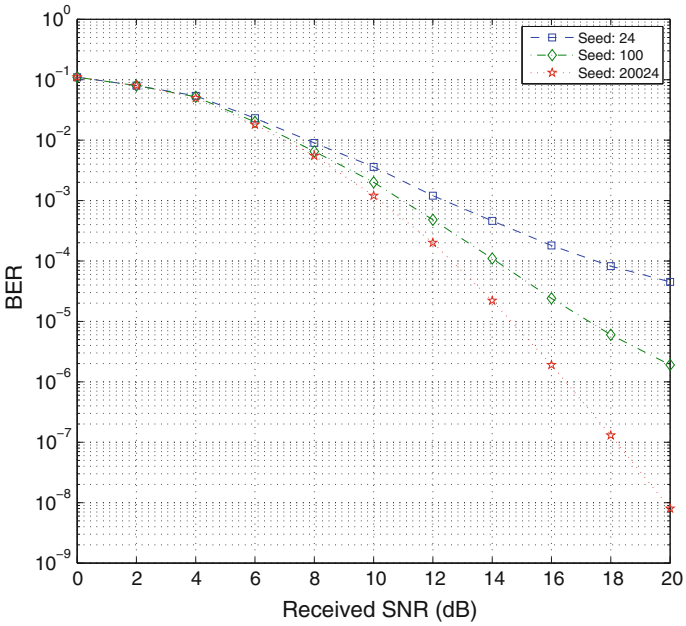

Fig. 7 Analytical BER performance curves produced by pseudo random user codes generated by different seeds for the same set of system and channel parameters ($K = 3$, $U = 1$, optimally spaced signaling)

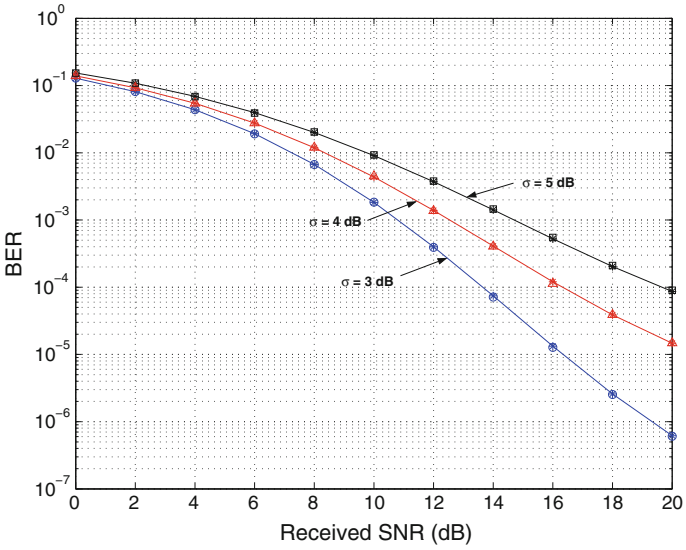

Fig. 8 Analytical and simulated (with *marker*) BER performance of the optimally spaced scheme with different channel standard deviation values ($K = 3$, $U = 1$)

system parameters chosen. This is easy to understand as a larger σ causes a higher amount of self-noise, which is clearly seen from (16).

Figure 9 shows the impact of channel RMS delay spread τ_{rms} on the performance of a single-user system ($K = 3$) with the optimally spaced signaling scheme. As expected, a

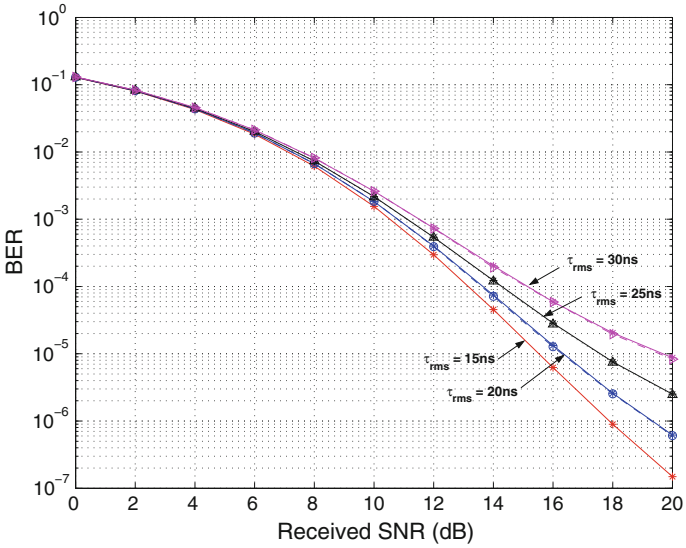

Fig. 9 BER performance for different channel delay spread values ($K = 3, U = 1$, optimally spaced signaling)

larger τ_{rms} value results in a higher BER under the same received SNR. At high SNR values, a larger τ_{rms} results in a higher error floor.

4.4 The Impact of Timing Jitter

For all examples so far we have assumed perfect symbol timing information in the receiver. Timing must be very accurate for pulsed UWB systems to achieve robust communications. In practical scenarios, timing jitter is typically on the order of 10 ps [20, 21] and can be modeled by a Gaussian or uniform distribution. We are interested in understanding how a DS-PPM system performs in the presence of timing jitter. Simulated BER curves of the optimally spaced scheme with $K = 2$ in the presence of different timing jitter values that are assumed to be uniformly distributed within a certain range are shown in Fig. 10. For comparison purposes, the error performance in the absence of timing jitter is also shown (solid line) in the same figure. There is approximately a 3.5 dB performance degradation at a BER of 10^{-4} when the jitter is uniformly distributed in the range -50 to 50 ps. For typical jitter values that are distributed in the range of -10 to 10 ps, the performance degradation is negligible compared to the ideal case (no timing jitter).

5 Conclusion

Through the analytical BER expression derived for a PPM UWB system with DS spreading for multiple access in a highly frequency-selective lognormal fading environment, we have quantified many critical performance metrics of DS-PPM UWB signaling such as the performance gain of optimally spaced signaling over orthogonal signaling, the impact of multipath delay spread and number of interfering users, performance degradation due to timing jitter, and the effect of different choices of user codes. With a typical set of system and channel parameters (e.g., those applied in examples in Sect. 4), the optimally spaced scheme could

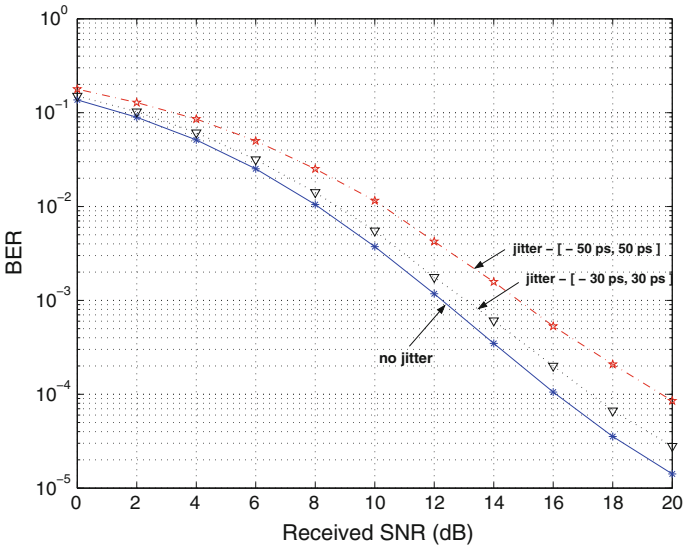

Fig. 10 Simulated BER performance curves in the presence of timing jitter ($K = 2$, $U = 1$, optimally spaced signaling)

outperform the orthogonal scheme by as much as 2 dB at a BER of 10^{-4}. Channel delay spread values have been found to significantly affect the BER performance. Timing jitters within practical ranges only slightly degrade the BER performance. The off-peak autocorrelation values of user codes, especially the values around the correlation peak, have significant impacts on the system performance as they determine the amount of self-noise.

References

1. Win, M., & Scholtz, R. (2000). Ultra-wide bandwidth timing-hopping spread spectrum impulse radio for wireless multiple-access communications. *IEEE Transactions on Communications, 48*, 36–38.
2. Durisi, G., & Benedetto, S. (2003). Performance evaluation and comparison of different modulation schemes for UWB multiaccess systems. In *Proceedings of IEEE ICC 2003* (pp. 2187–2191).
3. Foerster, J. R. (2002). The performance of a direct-sequence spread spectrum ultra-wideband system in the presence of multipath, narrowband interference and multiuser interference. In *Proceedings of the 2002 IEEE conference on ultra wideband systems and technologies* (pp. 87–91).
4. Wilson, R. D., & Scholtz, R. A. (2003). Comparison of CDMA and modulation schemes for UWB radio in a multipath environment. *Proceedings of IEEE Globecom'03* (pp. 754–758).
5. Guvenc, I., & Arslan, H. (2003). On the modulation options for UWB systems. In *Proceedings 2003 MILCOM*.
6. Ramirez-Mireles, F. (2002). Error probability of ultra wideband SSMA in a dense multipath environment. In *Proceedings of MILCOM 2002* (pp. 1081–1084).
7. Ge, L., Yue, G., & Affes, S. (2002). On the BER performance of pulse-position-modulation UWB radio in multipath channels. In *Proceedings of IEEE UWBST'02* (pp. 231–234).
8. Zhao, L., & Haimovich, A. M. (2002). Performance of ultra-wideband communications in the presence of interference. *IEEE Journal on Selected Areas in Communications, 20*, 1684–1691.
9. Somayazulu, V. S. (2002). Multiple access performance in UWB systems using time hopping vs. direct sequence spreading. *IEEE WCNC'02, 2*, 522–525.
10. Intel Research. (2002). Channel modeling sub-committee final report. In *IEEE P802.15 working group for wireless personal area networks*.
11. Cassioli, D., Win, M. Z., & Molisch, A. F. (2002). The ultra-wide bandwidth indoor channel: From statistical model to simulations. *IEEE Journal on Selected Areas in Communications, 20*, 1247–1257.

12. Molisch, A. F., Foerster, J. R., & Pendergrass, M. (2003). Channel models for ultra-wideband personal area networks. *IEEE Wireless Communications, 10*, 14–21.
13. Hashemi, H. (1993). Inpulse response modeling of indoor radio propagation channels. *IEEE Journal on Selected Areas in Communications, 11*, 967–978.
14. Scholtz, R. (1993). Multiple access with time-hopping impulse modulation. In *Proceedings of MILCOM'93* (Vol. 2, pp. 447–450).
15. Proakis, J. G. (1995). *Digital communications (Chap. 14)* (3rd ed.). New York, NY: McGraw-Hill.
16. Sabattini, M., Masry, E., & Milstein, L. B. (2003). A non-Gaussian approach to the performance analysis of UWB TH-BPPM systems. *IEEE UWBST'03*, 52–55.
17. Hu, B., & Beaulieu, N. C. (2003). Precise bit error rate of TH-PPM UWB systems in the presence of multiple access interference. *IEEE UWBS'03*, 106–110.
18. Durisi, G., & Romano, G. (2002). On the validity of Gaussian approximation to characterize the multiuser capacity of UWB TH PPM. In *Proceedings of IEEE UWBST'02* (pp. 157–161).
19. Foerster, J. R. (2001). The effects of multipath interference on the performance of UWB systems in an indoor wireless channel. In *Proceedings of IEEE VTC 2001–spring* (Vol. 2, pp. 1176–1180).
20. Tian, Z., & Giannakis, G. B. (2003). BER Sensitivity to mis-timing in correlation-based UWB receivers. In *Proceedings of IEEE global communications conference (Globecom'03)*.
21. Lovelace, W. M., & Townsend, J. K. (2002). The effects of timing jitter and tracking on the performance of impulse radio. *IEEE Journal on Selected Area in Communications, 20*, 1646–1651.
22. Molisch, A. F., Cassioli, D., Chong, C. C., Emami, S., Fort, A., & Kannan, B., et al. (2006). A comprehensive standardized model for ultrawideband propagation channels. *IEEE Transactions on Antennas and Propagation, 54*, 3151–3166.

Author Biographies

Mario E. Magaña (M'78–SM'94) received his B.S. degree in electrical engineering from Iowa State University in 1979, his MS degree in electrical engineering from the Georgia Institute of Technology in 1980, and his Ph.D., also in electrical Engineering, from Purdue University in 1987. He is currently an Associate Professor of Electrical Engineering and Computer Science at Oregon State University in Corvallis, Oregon, USA. He has also been an invited Researcher/Lecturer at the Universities of Ulm, Stuttgart, and Applied Sciences Offenburg, in Germany, and at the Technical University of Catalunya in Barcelona, Spain. He was also a Fulbright Professor at the National University of La Plata, Argentina. Prior to joining the faculty at Oregon State University in 1989 and before starting his doctoral studies at Purdue University, he spent several years working in the Analysis and Technology Group of the Communications Systems Division at the Harris Corporation in Melbourne, Florida, and in the Flight Control Systems Research Unit at the Boeing Company in Seattle, Washington. Dr. Magaña is a senior member of the IEEE, a NASA faculty fellow and a member of HKN, the electrical engineering honorary society. Finally, he is the author of more than 80 technical and scientific papers. His current areas of research are in the fields of mobile wireless communications, automatic control applications, signal processing, and mathematical modeling of biological systems.

Huaping Liu received the B.S. and M.S. degrees in electrical engineering from Nanjing University of Posts and Telecommunications, Nanjing, China, in 1987 and 1990, respectively, and the Ph.D. degree in electrical engineering from New Jersey Institute of Technology, Newark, in 1997. From July 1997 to August 2001, he was with Lucent Technologies, Whippany, NJ. Since September 2001, he has been with the School of Electrical Engineering and Computer Science, Oregon State University, Corvallis. His research interests include ultrawideband systems, multiple-input multiple-output antenna systems, channel coding, and modulation and detection techniques for multiuser communications. He is currently an Associate Editor for the IEEE Transactions on Vehicular Technology and IEEE Communications Letters, and an Editor for the Journal of Communications and Networks.

Vinod Venkatesan is currently a Sr. Staff Embedded DSP Engineer at Ikanos Communications Inc. previously Conexant Systems, Globespan Virata located at Redbank, New Jersey, USA. He received his B.E. degree in Instrumentation & Control Engineering from University of Madras, India in 2001 and his M.S. degree in Electrical Engineering & Computer Science from Oregon State University, USA in 2004.